PERGAMON

International Journal of Multiphase Flow 26 (2000) 1755–1769

International Journal of Multiphase Flow

www.elsevier.com/locate/ijmulflow

Interfacial friction in gas–liquid annular flow: analogies to full and transition roughness

L.B. Fore*, S.G. Beus, R.C. Bauer

Bettis Atomic Power Laboratory, Bechtel Bettis, Inc., West Mifflin, PA 15122, USA

Received 31 March 1999; received in revised form 23 November 1999

Abstract

New film thickness and pressure gradient data were obtained in a 5.08×101.6 mm duct for nitrogen and water in cocurrent upward annular flow. Pressures of 3.4 and 17 atm and temperatures of 38 and 93°C were used to vary the gas density between 4 and 20 kg/m^3 and liquid viscosity between 0.3×10^{-3} and 0.7×10^{-3} kg/m s. These data are used to compute interfacial shear stresses and interfacial friction factors for comparison with several accepted literature correlations. These comparisons are reasonable for small values of the relative film thickness. However, the new data cover conditions not approached by the data used to construct those correlations. By combining the current data with the results of two other comprehensive modern experimental studies, a new correlation for the interfacial friction factor has been developed. This correlation adds elements of transition roughness to Wallis' fully-rough analogy to better predict interfacial friction factors over a wide range of gas Reynolds numbers and liquid film thicknesses.

Keywords: Annular flow; Two-phase flow; Friction factors

1. Introduction

Gas–liquid annular flow is one of the most common two-phase flow patterns that arise in practice. It is characterized by a thin liquid film distributed around the perimeter of a conduit, with a mixture of gas and droplets in the core region of the conduit. The presence of the liquid film and droplets modify the gas velocity profile from the flattened profile expected in single-

* Corresponding author.

0301-9322/00/$ - see front matter
PII: S0301-9322(99)00114-7

phase turbulent flow to a more center-peaked profile (Gill et al., 1964; Jayawardena, 1993; Azzopardi and Teixeira, 1994). The power-law coefficient of the velocity profile, defined as n in

$$\frac{u}{u_c} = \left(\frac{2y}{D}\right)^{1/n}, \tag{1}$$

where u is the axial velocity, u_c is the axial velocity at the centerline, y is the distance from the wall and D is the conduit diameter, can be significantly smaller than the typical single-phase value of $n = 7$ for smooth conduits. This corresponds to a larger friction factor, f, than for the analogous single-phase flow, since

$$f \approx \frac{1}{4n^2} \tag{2}$$

according to Nunner's results (Hinze, 1975). When the friction velocity, u^*, is used to normalize the velocity profile in the velocity-defect law,

$$\frac{u_c - u}{u^*} = \frac{1}{\kappa} \ln\left(\frac{2y}{D}\right), \tag{3}$$

a smaller value of the von Karman constant, κ, is also found. Single-phase turbulent flow in rough tubes exhibits these same characteristics, with roughness decreasing the power-law coefficient and von Karman constant while increasing the friction factor and pressure drop.

Since pressure drop is one of the most important parameters used to characterize a flow system, several methods have been proposed to model or correlate the interfacial friction factor, f_i, in annular flow. Wallis (1969) suggested a correlation which treats the liquid film as a type of wall roughness. He originally fit four sets of annular flow data using the ratio of mean film thickness, h, to conduit hydraulic diameter with the relation

$$f_i = 0.005\left(1 + 300\frac{h}{D}\right). \tag{4}$$

He then noted the similarity to the relationship,

$$f = 0.005\left(1 + 75\frac{k_s}{D}\right), \tag{5}$$

where k_s is the Nikuradse sand-grain roughness height. The relationship (5) approximates the behavior of fully rough friction factors for values of k_s/D less than approximately 0.03. This result implied that the sand-grain roughness was approximately four times the mean film thickness for the conditions used to construct the correlation.

The Wallis correlation has been modified over the years, with some finding a better fit to data by using a computed single-phase gas friction factor, f_G, in place of the constant 0.005, as

$$f_i = f_G\left(1 + 300\frac{h}{D}\right). \tag{6}$$

However, this relationship no longer approximates fully rough friction factors, which should be

independent of the gas Reynolds number, Re_G, from which f_G is calculated. Additionally, neither Eqs. (4) nor (6) accurately predicts the behavior of thicker films in a number of studies reported in the literature. Various explanations have been suggested for the deviation at large film thicknesses. For several studies, the larger film thicknesses correspond to smaller gas flow rates and corresponding gas Reynolds numbers (Asali, 1984; Zabaras et al., 1986; Fore and Dukler, 1995a; Fukano and Furukawa, 1998). This fact, and some analysis of Zabaras (1985) film thickness and pressure drop data, led Lopes and Dukler (1986) to suggest transition roughness, as opposed to full roughness, as the mechanism for the enhanced friction factor at smaller gas Reynolds numbers and larger film thicknesses. To this point, however, this idea has not been pursued substantially further.

Several correlations have been proposed to better predict the behavior of the friction factors for large film thicknesses that has sometimes been observed. Henstock and Hanratty (1976) and Asali et al. (1985) developed correlations to account for the deviation of some measured friction factors from the Wallis, or modified Wallis, correlation. Practically all of the data used to develop these correlations were obtained under relatively low pressures. This paper presents new measurements obtained at higher pressures which can be used in conjunction with existing published data to better understand and account for the behavior of the interfacial friction factor at low Reynolds numbers. A new correlation is developed, based on the analogy to transition roughness, to obtain better predictions over a fuller range of Reynolds numbers than represented by existing correlations.

2. Experimental

2.1. Flow loop

Fig. 1 is a schematic of the test section and flow loop used to obtain the new measurements presented in this paper. Both gas and liquid flow systems were operated as closed loops. A large separator tank was used as a loop pressurizer and as the reservoir for gas and liquid. A centrifugal pump was used to circulate water from the separator, through a pair of Endress-Hauser Promass model 63F Coriolis flow meters installed in series, and to the test section liquid entry section. A reciprocating compressor was used to circulate nitrogen from the separator, through a pair of Rosemount Model 8800 vortex flow meters installed in series, and to the test section gas inlet piping. The manufacturer-stated accuracies of the water and gas flow meters were ± 2 and $\pm 1\%$, respectively. A gas heater was used to control the nitrogen temperature and several water heaters were used to control the water temperature. The system pressure was controlled by a pressure-regulated nitrogen supply attached to the top portion of the loop separator. Temperatures, measured with chromel-alumel thermocouples, are considered accurate within $\pm 2^{\circ}C$ and system gage pressures, measured with Rosemount Model 3051C pressure transmitters, are considered accurate within $\pm 1\%$.

2.2. Test section and measurement techniques

The test section was a 5.08 × 101.6 mm by 3.4-m-long rectangular duct constructed of 304

stainless steel. The liquid feed in the test section was made up of two porous sections of the side walls and the gas feed was made up of an axial length of piping attached to the bottom of the test section. The gas and liquid exited through two porous wall sections near the top of the test section and through an axial length of piping attached to the top of the test section. Three pairs of fused-silica windows, including one large pair, were installed in the test section for flow observation. All measurements, as described below, were made between the liquid entry section and the pair of large observation windows.

Pressure taps were located at nine locations between the liquid entry section and the observation window along a vertical line displaced 2.54 cm from the center of the 101.6 mm wide wall. The tap locations were at positions 10.8, 28.6, 46.4, 64.0, 81.9, 99.7, 117.5, 135.3 and 153 cm above the liquid entry section. Eight pressure drop measurements were made with Rosemount Model 3051C differential pressure transmitters between the lowest pressure tap and each of the taps located above it (from 10.8 to 28.6 cm, 10.8 to 46.4 cm, etc.). Each of these measurements is considered accurate within $\pm 1\%$. All differential pressures were digitized at three samples per second and digitally filtered to smooth out the time-dependent fluctuations. The time required to reach steady time-smoothed values of differential pressure depended on flow conditions. The time series of

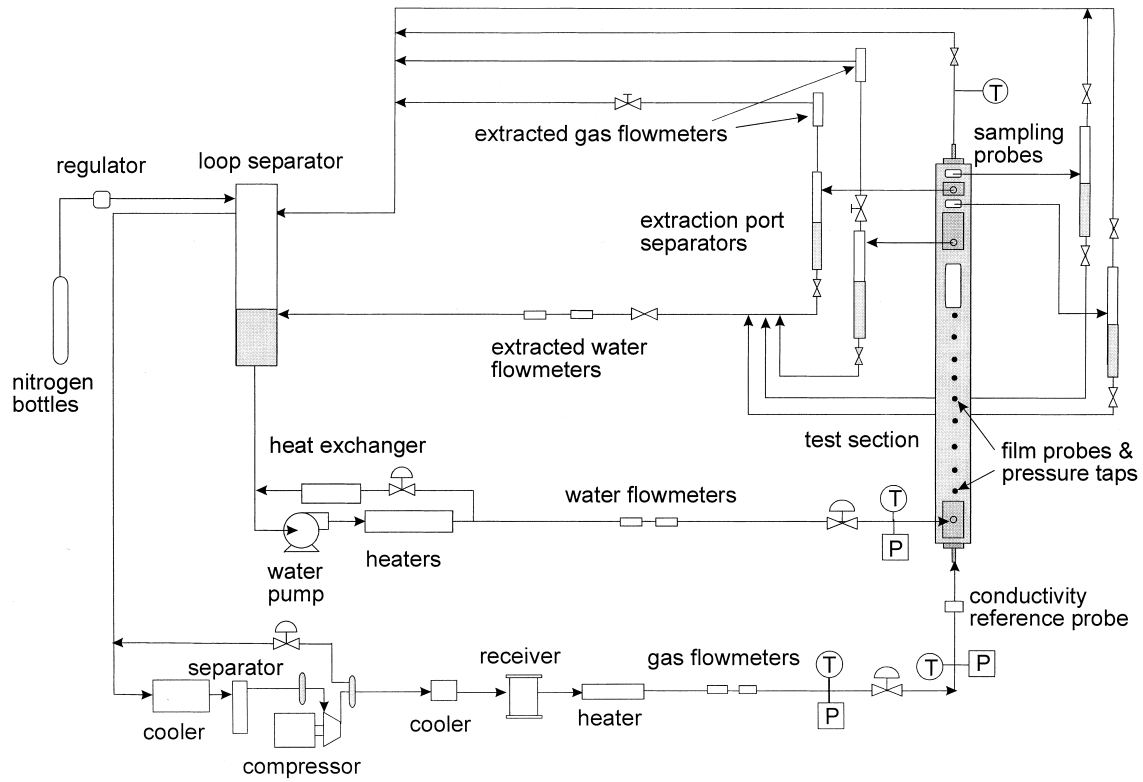

Fig. 1. Nitrogen–water flow loop and test section.

the smoothed differential pressures were observed until they reached steady values, at which time each was recorded to disk along with the flow rates, miscellaneous temperatures and system gage pressures.

Film thickness probes were located at the same axial locations as the pressure taps along a vertical line at the center of the 101.6 mm side wall. The film thickness probes were constructed of 6.35 mm diameter cylindrical Teflon inserts with 1.59 mm diameter chromel wires imbedded along the insert axis to form a coaxial conductor–insulator arrangement mounted flush with the test section wall. The conductance of the liquid film above the probes and between the face of the chromel wire and the test section wall was measured with a circuit similar to that described by Coney (1973) and related to the film thickness through a calibration. A conductivity reference probe was installed in the liquid lines leading to the test section and used to compensate for temperature and concentration-dependent variations in electrical conductivity. More accurate film thickness measurements are possible with conductance probes mounted flush with a flat surface as opposed to the curved surface of a small diameter tube. This is mainly the result of an increase in calibration accuracy. Typically, liquid films of varying thickness are simulated by the positioning of a non-conductive surface parallel to the test section wall above a flush-mounted film thickness probe. In tubular test sections, a separate machined rod for each discrete film thickness is used to form the second surface for the calibration (Asali, 1984). Various factors, including machining tolerances and thermal expansion, add some uncertainty to the magnitude of the gap between the machined rod and the tube wall. With the flat wall in the current study, a single non-conductive parallel surface was positioned with a micrometer to form a large number of precisely measured gaps down to 0.02 mm. This level of calibration accuracy was necessary, since liquid films as thin as 0.05 mm were present under some conditions. Assuming the conductivity variation is properly accounted for, the calibration accuracy of ± 0.02 mm represents a best-case estimate of the accuracy of a single film thickness probe.

The output voltages of the conditioning circuit for eight of the nine film probes (all probes except that located at 81.9 cm) and the conductivity reference probe were digitized at 2000 samples per second for 60 s. The output voltages were converted to film thickness and a mean value was calculated for each probe. Since the mean film thickness did not vary systematically from probe to probe, the mean values associated with the upper seven probes were averaged together to reduce the uncertainty associated with an individual film thickness probe measurement.

The entrained liquid fraction was estimated by withdrawing the liquid film through a porous wall section located above the ninth film thickness probe and collecting the entrained droplets with a traversing sampling probe of diameter 1.57 mm similar to that used by Asali (1984). The deposition rate was estimated by repeating this measurement with a second traversing probe located 0.307 m downstream. The reduction of droplet flow from the first probe to the second is directly related to the deposition rate of the droplets onto the wall. Neither of the two sampling probes was operated in an isokinetic manner, which has been shown to be unnecessary by Asali (1984) and others for the measurement of annular flow droplet flux (Wicks and Dukler, 1960; Gill et al., 1963). The accuracies of the entrained fraction and deposition rate measurement were estimated at ± 5 and $\pm 10\%$, respectively.

2.3. Test conditions

Film thickness and pressure gradient data were collected for nitrogen–water annular flow at 136 different operating conditions. Two nominal system pressures, 3.4 and 17 atm, and two nominal temperatures, 38 and 93°C were used to produce four nominal pressure–temperature combinations. The actual pressure in the test section, which differed from the nominal value due to the pressure drop, was used to estimate gas physical properties. The gas density varied between 3.4 and 20 kg/m^3 while the liquid viscosity varied between 0.3×10^{-3} and 0.7×10^{-3} kg/m s. The range of superficial gas velocity at each temperature was 5 to 30 m/s at $p = 3.4$ atm and 4 to 20 m/s at $p = 17$ atm. The range of superficial liquid velocity was 0.06 to 1.0 m/s for all combinations of pressure and temperature. The combinations of temperature, pressure and flow rates produced a range of liquid Reynolds numbers between 800 and 32,000 and gas Reynolds numbers between 8300 and 182,000. Table 1 contains the liquid viscosity, range of gas density and ranges of liquid and gas Reynolds numbers for each nominal condition.

3. Momentum balance analysis and friction factors

The interfacial friction factor in annular flow is typically defined by

$$f_i = \frac{2\tau_i}{\rho_G U_G^2}, \tag{7}$$

where τ_i is the interfacial shear stress, ρ_G is the gas density and U_G is the mean gas velocity in the gas-droplet core. In some cases, the core gas-droplet density and the superficial gas velocity have been used in an alternate definition of the interfacial friction factor. The interfacial shear stress is computed with a momentum balance applied in the axial direction on the gas-droplet core (Moeck and Stachiewicz, 1972; Lopes and Dukler, 1986; Fore and Dukler, 1995a). For some data in the open literature, significant gas expansion was present, which affects the entrainment process and accounts for some fraction of the total pressure drop (Cousins et al., 1965). Neglecting this effect adds a positive bias to the computed value of the interfacial shear stress and to the interfacial friction factor. The following momentum balance analysis is

Table 1
Physical properties and range of Reynolds numbers for current data

Nominal conditions		Liquid viscosity (kg/m s $\times 10^3$)	Gas density range (kg/m^3)	Liquid Reynolds number range	Gas Reynolds number range
P (atm)	T (°C)				
3.4	38	0.7	3.8–5.9	800–15,000	11,000–67,000
3.4	93	0.3	3.4–5.0	1500–32,000	8300–54,000
17	38	0.7	18.9–19.9	800–15,000	53,000–182,000
17	93	0.3	16.3–17.8	1500–32,000	33,000–145,000

slightly different from those presented by Lopes and Dukler and Fore and Dukler, in that an estimate of the gas expansion effect is included.

Fig. 2 is a schematic of the gas-droplet core of a typical adiabatic annular flow. The control volume used for the momentum balance is bounded by the film on the sides parallel to the axial direction and by planes spaced an arbitrary distance apart normal to the axial direction. At steady state, a momentum balance in the axial direction, z, over this control volume is written

$$\int_A u_z \rho_c u_z \, dA = \int_A T_z \, dA + \int_V B_z \, dV, \tag{8}$$

where u_z is the local axial velocity, ρ_c is the core mixture density, T_z is the axially-directed surface force per unit area and B_z is the axial body force per unit volume.

Under true equilibrium conditions, the convective integral on the left-hand side of Eq. (8) consists solely of the momentum changes caused by the entrainment-deposition process, in which faster moving drops deposit out of the control volume and slower moving drops entrain

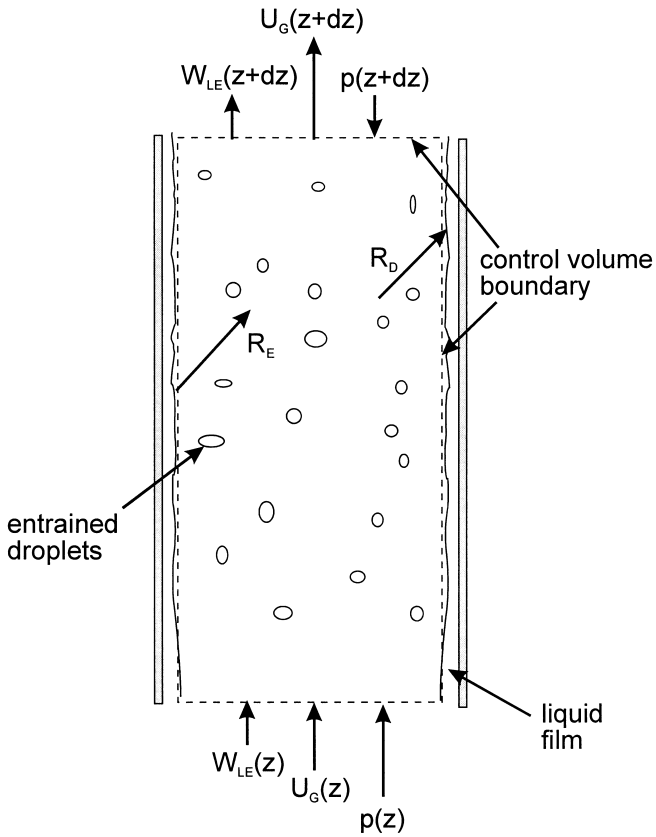

Fig. 2. Control volume for momentum transfer analysis.

into the control volume. When there is significant gas expansion or a change in entrainment within the control volume, another term is added to the convective integral. Using A_c as the cross sectional area of the control volume and P_c as the perimeter, the convective integral can be approximated as

$$\int_A u_z \rho_c u_z \, dA = A_c d\left(\rho_c U_z^2\right) + P_c \, dz (R_D U_D - R_E U_E), \tag{9}$$

where R_E is the entrainment rate, R_D is the deposition rate, U_z is the mean axial velocity in the control volume, U_E is the mean axial velocity of entraining drops and U_D is the mean axial velocity of depositing drops. The surface force integral contains the interfacial shear stress, τ_i, and applied pressure, p, while the body force integral contains the force on the gas and droplets caused by the gravitational acceleration, g, as

$$\int_A T_z \, dA = -P_c \, dz \tau_i - A_c \, dp \tag{10}$$

and

$$\int_V B_z \, dV = -A_c \, dz \rho_c g. \tag{11}$$

Combining and simplifying the various terms results in

$$\tau_i = -\frac{A_c}{P_c}\left(\frac{dp}{dz} + \frac{d}{dz}\left(\rho_c U_z^2\right) + \rho_c g\right) - R_D U_D + R_E U_E. \tag{12}$$

The axial derivative of the axial momentum flux, $\rho_c U_z^2$, can be evaluated with a few assumptions, using the definition

$$\rho_c U_z A_c = W_G + W_{LE}, \tag{13}$$

where W_G is the gas mass flow rate and W_{LE} is the entrainment mass flow rate. Without evaporation or condensation, W_G is constant but W_{LE} can still vary due to non-equilibrium entrainment-deposition conditions. The derivative of the total axial momentum can then be evaluated as

$$\frac{d}{dz}\left(\rho_c U_z^2 A_c\right) = \frac{d}{dz}\left[(W_G + W_{LE}) U_z\right] = W_G \frac{dU_z}{dz} + W_{LE} \frac{dU_z}{dz} + U_z \frac{dW_{LE}}{dz}. \tag{14}$$

The axial derivative of the velocity can be evaluated with the pressure gradient, assuming that the droplets and gas travel at approximately the same velocity and that the gas follows the ideal gas law, with the density directly proportional to pressure, as

$$\frac{dU_z}{dz} = -U_G \frac{dp/dz}{p}. \tag{15}$$

Eq. (14) can then be simplified to

$$\frac{\mathrm{d}}{\mathrm{d}z}\left(\rho_{\mathrm{c}} U_z^2 A_{\mathrm{c}}\right) = -\rho_{\mathrm{c}} U_{\mathrm{G}}^2 A_{\mathrm{c}} \frac{\mathrm{d}p/\mathrm{d}z}{p} + U_{\mathrm{G}} \frac{\mathrm{d}W_{\mathrm{LE}}}{\mathrm{d}z}. \tag{16}$$

For the special case of equilibrium annular flow, where deposition and entrainment rates are equal and the entrainment flow rate is unchanging with distance, the equation for the interfacial shear stress simplifies to

$$\tau_{\mathrm{i}} = -\frac{A_{\mathrm{c}}}{P_{\mathrm{c}}}\left[\frac{\mathrm{d}p}{\mathrm{d}z}\left(1 - \frac{\rho_{\mathrm{c}} U_{\mathrm{G}}^2}{p}\right) + \rho_{\mathrm{c}} g\right] - R_{\mathrm{D}}(U_{\mathrm{D}} - U_{\mathrm{E}}). \tag{17}$$

4. Correlation of friction factors

The interfacial shear stress was calculated for the current set of data, as well as the data of Fore and Dukler (1995a) and Asali (1984) in order to make the following comparisons and analysis. Table 2 is a brief description of the test section size, geometry and system pressure for the data used from these three studies. The current set of data complements the previous data described in the table through an increase of system pressure and a change of geometry. For both this set of data and the Fore and Dukler data, only conditions visually observed to be within the disturbance-wave regime of annular flow are used. The disturbance-wave regime is characterized by large waves on the liquid film which travel upward at a relatively constant velocity and can be observed over an appreciable distance. In the film-churning regime, which can occur at lower gas velocities, large liquid lumps exhibit an up-and-down motion on the film and do not travel over a significant distance before disappearing by coalescence or breakup. Due to the different physical behavior, the same mechanisms for interfacial shear stress may not apply to both the disturbance-wave and film-churning regimes.

The pressure gradient and film thickness were measured in all three studies listed in Table 2. The entrained fraction and deposition rate were measured in the current and Fore and Dukler studies, while only the entrained fraction was measured by Asali. For the Asali data sets, the deposition rate was estimated using Leman's (1985) correlation, which was developed from data obtained in the same experimental setup. The entraining droplet velocity, U_{E}, was taken

Table 2
Data sets used for comparison

Study	Gas/liquid system	Geometry and size (mm)	Pressure (atm)	Temperature (°C)
Current	Nitrogen–water	Duct, 5.08 × 101.6	3.4	38 and 93
Current	Nitrogen–water	Duct, 5.08 × 101.6	17	38 and 93
Fore and Dukler (1995a)	Air–water	Tube, 50.8	1	18
Fore and Dukler (1995a)	Air–50% water/glycerine	Tube, 50.8	1	18
Asali (1984)	Air–water	Tube, 22.9	1	21
Asali (1984)	Air–water	Tube, 42	1	21
Asali (1984)	Air–water	Tube, 42	2	21

as the wave velocity, for the current and Fore and Dukler (1995a) studies in which it was measured, and as twice the mean liquid film velocity, for the Asali (1984) study. The depositing droplet velocity, U_D, was taken as 80% of the mean gas velocity, based on the experimental gas and droplet velocities of Fore and Dukler (1995b) and Azzopardi and Teixeira (1994).

Fig. 3 is a comparison of the data summarized in Table 2 with the original Wallis friction factor shown in Eq. (5). The current data at both pressures of 3.4 and 17 atm agree with the Fore and Dukler (1995a) and Asali (1984) data for relative film thicknesses, h/D, below about 0.01. All of the lower pressure data, including the current data obtained at a pressure of 3.4 atm, deviate from the Wallis correlation as the value of h/D increases. Significantly, the current data obtained at a pressure of 17 atm agree well with the Wallis correlation over the full upper range of relative film thickness between 0.01 and 0.04. Like the original four data sets used to construct the Wallis correlation, all of the friction factors, including the current data, are overpredicted for very small values of the relative film thickness, h/D. However, a simple shift in h/D introduced in the original correlation as

$$f_i = 0.005\left[1 + 300\left(\frac{h}{D} - 0.0015\right)\right] \tag{18}$$

can account for this difference. A justification for this small modification may be that a finite relative film thickness is needed before a significant change to the smooth friction factors is observed. A similar term was included in the Asali et al. (1985) correlation as outlined below.

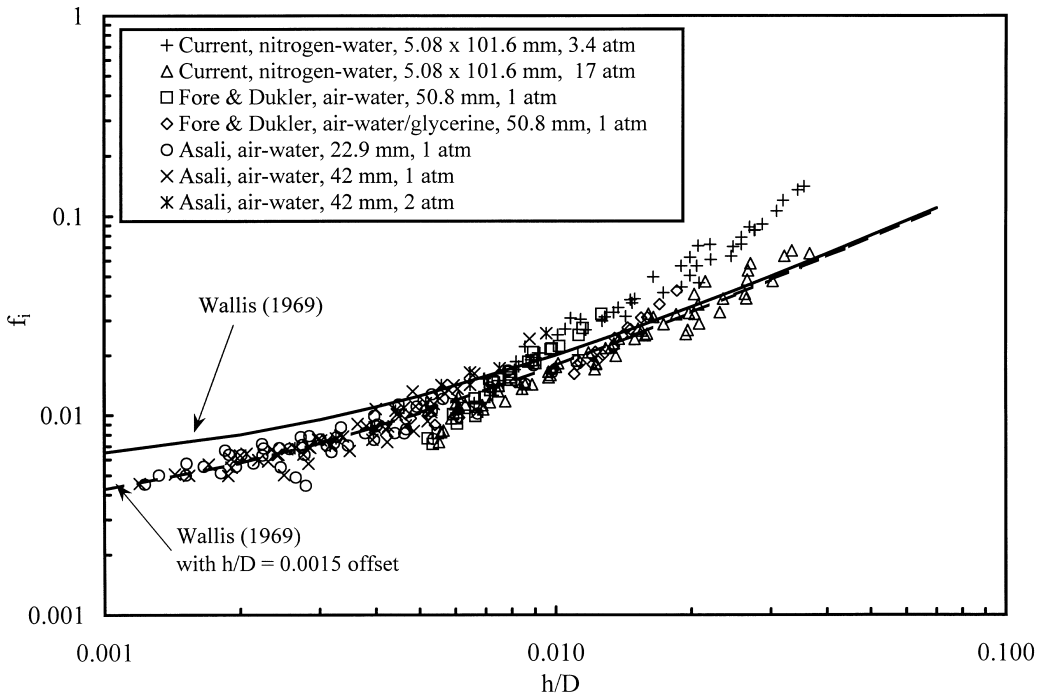

Fig. 3. Comparison of computed friction factors with Wallis (1969) correlation.

Henstock and Hanratty (1976) used a parameter, F, to fit several sets of friction factor data with the two equations,

$$\frac{h}{D} = \frac{6.59F}{\sqrt{f_i/f_G}} \tag{19}$$

and

$$\frac{f_i}{f_G} = 1 + 1400F, \tag{20}$$

which can be combined to yield a form similar to the modified Wallis correlation (6) as

$$f_i = f_G\left(1 + 212\sqrt{\frac{f_i}{f_G}}\frac{h}{D}\right). \tag{21}$$

The current set of data and the others listed in Table 2 are compared to this correlation in Fig. 4. While the Henstock and Hanratty correlation reflects the behavior of some of the lower pressure data at large film thicknesses, it severely overpredicts the friction factors at higher pressure.

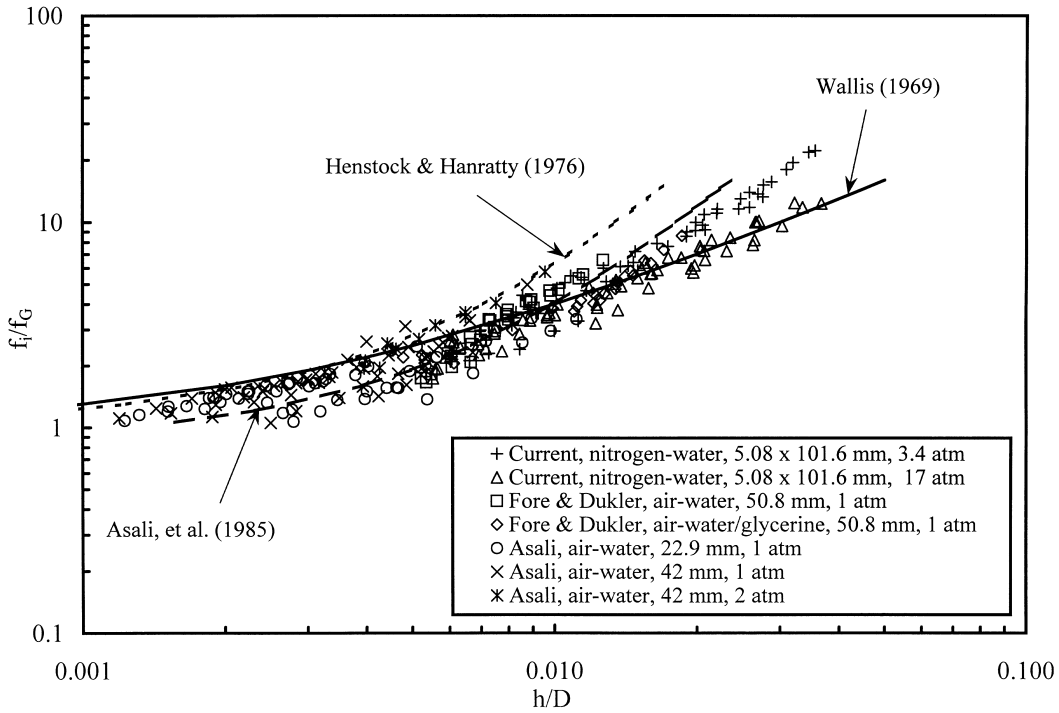

Fig. 4. Comparison of computed friction factors with Henstock and Hanratty (1976) and Asali et al. (1985) correlations.

Asali et al. (1985) used additional data obtained from Asali (1984) to build a slightly different friction factor correlation as

$$\frac{f_i}{f_G} = 1 + 0.45 Re_G^{-0.2}\left(Re_G\sqrt{\frac{f_i}{2}}\frac{h}{D} - 4\right). \tag{22}$$

The constant, 4, within the parentheses is used to approximate the thickness of the laminar sublayer in wall coordinates. The hypothesis is that only films thicker than the laminar sublayer will increase the interfacial friction factor above the analogous single-phase value. The explicit dependence on the gas Reynolds number in Eq. (22) can be removed by using the relationship $f_G = 0.046 Re_G^{-}0.2$ to yield

$$f_i = f_G\left(1 + 1.46\times 10^{-7} f_G^{-7/2}\sqrt{\frac{f_i}{f_G}}\frac{h}{D} - 39.2 f_G\right), \tag{23}$$

which can be compared roughly to the Henstock and Hanratty correlation by substituting a nominal value of $f_G = 0.005$ for terms within the parentheses to yield the approximation

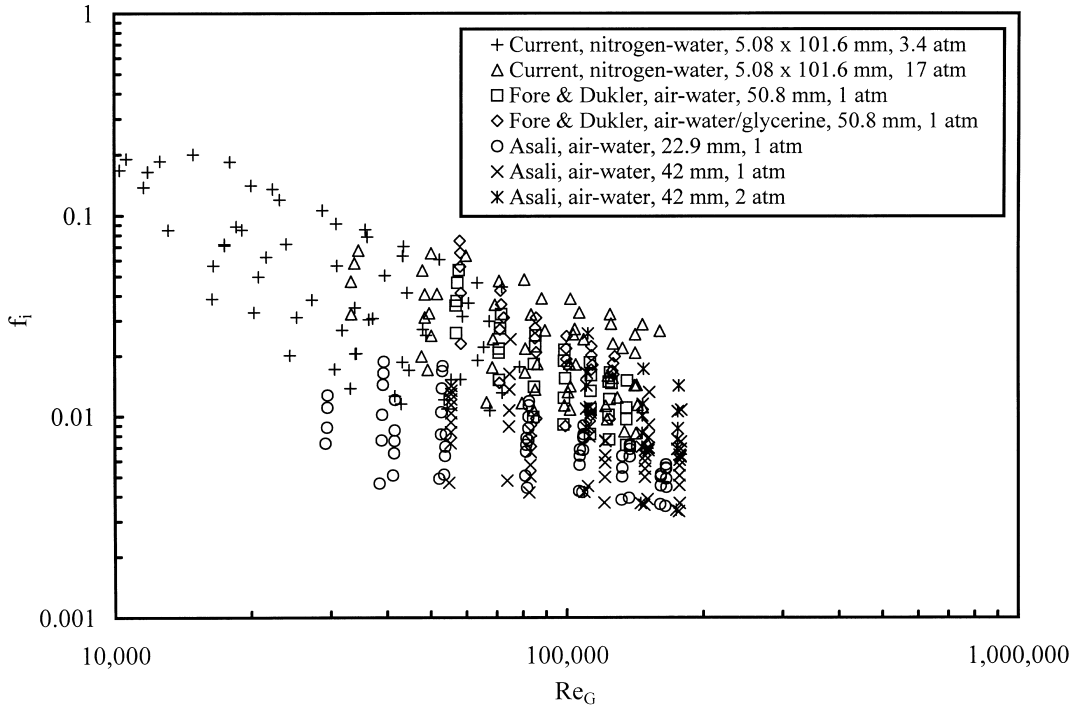

Fig. 5. Computed friction factors versus gas Reynolds number.

$$f_i = f_G\left(0.8 + 161\sqrt{\frac{f_i}{f_G}}\frac{h}{D}\right). \tag{24}$$

The three sets of data are also compared to this relationship in Fig. 4. Like the Henstock and Hanratty correlation, the Asali et al. correlation overpredicts the friction factors for large values of the relative film thickness. The agreement is best at low values of h/D, which is typical of the Asali (1984) data from which this correlation was developed.

The deviation of the interfacial friction factors from the fully-rough analogy represented by the Wallis correlation was suggested by Lopes and Dukler (1986) to be an effect of transition roughness. In single-phase flow, friction factors for transitionally-rough flows depend on both the roughness height and on the Reynolds number (cf.: Schlichting, 1979). Fig. 5 is a plot of the friction factors versus the gas Reynolds number for all of the data used in the above comparisons. Unlike the Lopes and Dukler result obtained with limited data, one curve cannot be used to represent all of these data.

In the transition region between smooth and fully-rough pipe flow, the friction factor decreases asymptotically with increasing Reynolds number to the relation shown in Eq. (5), which depends only on the relative roughness height. Since a similar decrease with Reynolds number is shown in Fig. 5 for annular flow, an interfacial friction factor correlation should also asymptotically approach a value dependent only on the analogous relative roughness

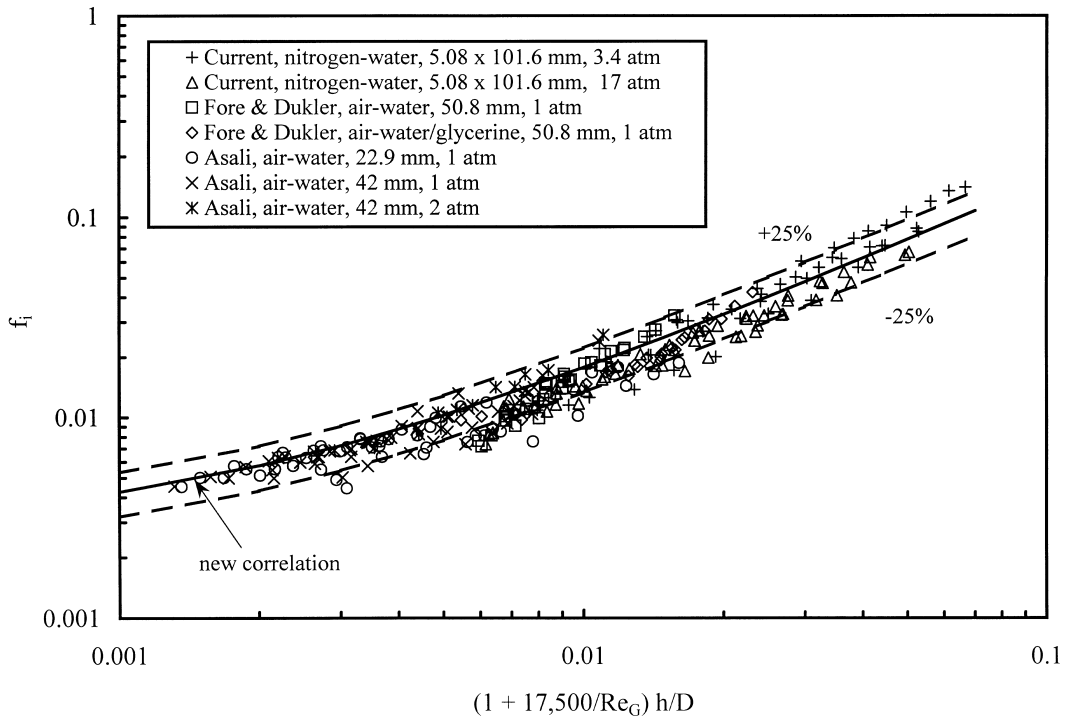

Fig. 6. Comparison of computed friction factors with new correlation.

height at large gas Reynolds numbers. However, classic friction factor relations for transition and full roughness do not adequately account for the Reynolds number dependence in annular flow. The simple multiplication factor, $(1 + A/Re_G)$, has been chosen for inclusion in an improved friction factor correlation to achieve a stronger dependence on the gas Reynolds number. In order to maintain the behavior of the Wallis correlation at small values of the relative film thickness, while incorporating some aspects of transition roughness, the new correlation,

$$f_i = 0.005\left\{1 + 300\left[\left(1 + \frac{17{,}500}{Re_G}\right)\frac{h}{D} - 0.0015\right]\right\}, \tag{25}$$

has been developed by using a best-fit value of $A = 17{,}500$. The gas Reynolds number in this equation is based on the core area and perimeter as

$$Re_G = \frac{\rho_G U_G (4A_C/P_C)}{\mu_G}, \tag{26}$$

where μ_G is the absolute viscosity of the gas. This definition differs slightly from the Reynolds number based on the hydraulic diameter of the conduit due to the reduction in flow area and perimeter by the presence of the liquid film. Analogous to the friction factors in rough pipes, Eq. (25) produces friction factors that depend only on h/D, or roughness by analogy, at large Reynolds numbers by reducing to Eq. (18) as Re_G approaches infinity. A comparison with this correlation is shown in Fig. 6 with 25% uncertainty bands. The agreement of all these data, which include more than 200 modern measurements taken in three different experimental studies, is better with this new correlation than with any of the three literature correlations evaluated in Figs. 3 and 4.

5. Conclusions

Interfacial friction factors obtained from new film thickness and pressure gradient measurements in cocurrent upward gas–liquid annular flow have been compared to three generally-accepted literature correlations and used to develop a new correlation. The new data, obtained in a 5.08 × 101.6 mm duct using nitrogen and water at pressures and temperatures in excess of 17 atm and 93°C, respectively, expand the ranges of gas density and liquid viscosity beyond the ranges used in constructing those three literature correlations of Wallis (1969), Henstock and Hanratty (1976) and Asali et al. (1985). Several observations and conclusions are detailed below.

1. Comparisons of the new data with the correlations of Wallis (1969), Henstock and Hanratty (1976) and Asali et al. (1985) are reasonable for small values of the relative film thickness, h/D.
2. As the magnitude of the relative film thickness increases, the new friction factors obtained at a lower nominal pressure of 3.4 atm deviate from the Wallis correlation in a manner similar to that observed in other data (Asali, 1984; Zabaras et al., 1986; Fore and Dukler, 1995a). However, the new friction factors obtained at the higher nominal pressure of 17 atm

maintain agreement with the Wallis correlation at the largest measured relative film thicknesses.

3. Using Lopes and Dukler (1986) supposition that transition roughness causes the interfacial friction factor to deviate from the Wallis correlation, which is based on a fully-rough analogy, a new correlation has been developed. This correlation adds a dependence on the gas Reynolds number to the Wallis correlation to approximate the effects of transition roughness and better predict the interfacial friction factor at large relative film thicknesses and small gas Reynolds numbers.

References

Asali, J.C., 1984. Entrainment in vertical gas–liquid annular flows. Ph.D. Dissertation, University of Illinois.

Asali, J.C., Hanratty, T.J., Andreussi, P., 1985. Interfacial dag and film height for vertical annular flow. AIChE J. 31, 895–902.

Azzopardi, B.J., Teixeira, J.C.F., 1994. Detailed measurements of vertical annular two-phase flow. Part II: gas core turbulence. Trans. ASME: J. Fluids Eng. 116, 796–800.

Coney, M.W.E., 1973. The theory and application of conductance probes for the measurement of liquid film in two-phase flow. J. Phys. E: Scientific Instruments 6, 903–910.

Cousins, L.B., Denton, W.H., Hewitt, G.F., 1965. Liquid mass transfer in annular two-phase flow. In: Symposium on Two-Phase Flow (Paper C4), University of Exeter, vol. 2, C401–C430.

Fore, L.B., Dukler, A.E., 1995a. Droplet deposition and momentum transfer in annular flow. AIChE J. 41, 2040–2046.

Fore, L.B., Dukler, A.E., 1995b. The distribution of drop size and velocity in gas–liquid annular flow. Int. J. Multiphase Flow 21, 137–149.

Fukano, T., Furukawa, T., 1998. Prediction of the effects of liquid viscosity on interfacial shear stress and frictional pressure drop in vertical upward gas–liquid annular flow. Int. J. Multiphase Flow 24, 587–603.

Gill, L.E., Hewitt, G.F., Hitchon, J.W., Lacey, P.M.C., 1963. Sampling probe studies of the gas core in annular two-phase flow. Part I: the effect of length on the phase and velocity distribution. Chem. Eng. Sci. 18, 525–535.

Gill, L.E., Hewitt, G.F., Lacey, P.M.C., 1964. Sampling probe studies of the gas core in annular two-phase flow. Part II: studies of the effect of phase flow rates on phase and velocity distribution. Chem. Eng. Sci. 19, 665–682.

Henstock, W.H., Hanratty, T.J., 1976. The interfacial drag and the height of the wall layer in annular flows. AIChE J. 22, 990–1000.

Hinze, J.O., 1975. Turbulence, 2nd ed. McGraw-Hill, New York.

Jayawardena, S.S., 1993. Turbulent flow in the core region of vertical annular gas-liquid flow. Ph.D. Dissertation, University of Houston.

Leman, G.W., 1985. Atomization and deposition in two-phase annular flow: Measurement and modeling. Ph.D. Dissertation, University of Illinois.

Lopes, J.C.B., Dukler, A.E., 1986. Droplet entrainment in vertical annular flow and its contribution to momentum transfer. AIChE J. 32, 1500–1515.

Moeck, E.O., Stachiewicz, J.W., 1972. A droplet interchange model for annular-dispersed, two-phase flow. Int. J. Heat Mass Transfer 15, 637–653.

Schlichting, H., 1979. Boundary-Layer Theory, 7th ed. McGraw-Hill, New York.

Wallis, G.B., 1969. One Dimensional Two-Phase Flow. McGraw-Hill, New York.

Wicks, M., Dukler, A.E., 1960. Entrainment and pressure drop in concurrent gas-liquid flow: air–water in horizontal flow. AIChE J. 6, 463–468.

Zabaras, G.J., 1985. Studies of vertical annular gas–liquid flows. Ph.D. Dissertation, University of Houston.

Zabaras, G.J., Dukler, A.E., Moalem-Maron, D., 1986. Vertical upward cocurrent gas–liquid annular flow. AIChE J. 32, 829–843.